Published in final edited form as:
Biochemistry. 2010 December 21; 49(50): 10666–10673. doi:10.1021/bi1013485.

Cellular Uptake of Ribonuclease A Relies on Anionic Glycans†

Tzu-Yuan Chao[‡], **Luke D. Lavis**[#,§], and **Ronald T. Raines**[*,‡,#]

[‡]Department of Biochemistry, University of Wisconsin–Madison, Madison, Wisconsin 53706

[#]Department of Chemistry, University of Wisconsin–Madison, Madison, Wisconsin 53706

Abstract

Bovine pancreatic ribonuclease (RNase A) can enter human cells, even though it lacks a cognate cell-surface receptor protein. Here, we report on the biochemical basis for its cellular uptake. Analyses *in vitro* and *in cellulo* revealed that RNase A interacts tightly with abundant cell-surface proteoglycans containing glycosaminoglycans, such as heparan sulfate and chondroitin sulfate, as well as with sialic acid-containing glycoproteins. The uptake of RNase A correlates with cell anionicity, as quantified by measuring electrophoretic mobility. The cellular binding and uptake of RNase A contrast with those of Onconase®, an amphibian homologue that does not interact tightly with anionic cell-surface glycans. As anionic glycans are especially abundant on human tumor cells, our data predicate utility for mammalian ribonucleases as cancer chemotherapeutic agents.

Cancer has been the second leading cause of death in the U.S. since 1935. As a consequence, tremendous efforts have been devoted to the development of anticancer agents with a high efficacy and therapeutic index. Traditional cancer chemotherapy is based on small molecules that target DNA synthesis and transcription (1). Newer small-molecule and monoclonal antibody-based anticancer drugs interfere with the function of a wider variety of proteins (2). The use of oligonucleotides or derivatives to target RNA is another strategy, but one that now suffers from inefficient delivery (3). The pancreatic-type ribonucleases represent a novel class of cancer chemotherapeutic agent that interrupts the flow of genetic information at the RNA level. One such ribonuclease, Onconase® (ONC1 (4)) from the Northern leopard frog, is on the verge of approval as a chemotherapeutic agent for malignant mesothelioma, and has orphan-drug and fast-track status.

Surprisingly, bovine pancreatic ribonuclease (RNase A (5); EC 3.1.27.5) is not cytotoxic, despite being homologous to ONC. Unlike ONC, RNase A binds with femtomolar affinity to the cytosolic ribonuclease inhibitor protein (RI (6)). This protein likely evolved to sequester secretory ribonucleases that invade mammalian cells. Variants of RNase A that evade RI are cytotoxic *in vitro* (7–9) and *in vivo* (10). One such variant, D38R/R39D/N67R/G88R RNase A (DRNG RNase A), contains four amino-acid substitutions that disrupt shape complementarity within the RI–RNase A interface, resulting in a 2×10^6-fold increase in the

†This work was supported by Grant R01 CA073808 (NIH). T.-Y.C. was supported by the Dr. James Chieh-Hsia Mao Wisconsin Distinguished Graduate Fellowship. L.D.L was supported by Biotechnology Training Grant T32 08349 (NIH) and an ACS Division of Organic Chemistry Fellowship sponsored by Genentech. The Biophysics Instrumentation Facility was established with Grants BIR-9512577 (NSF) and S10 RR013790 (NIH).

[*]Address correspondence to: Ronald T. Raines, Department of Biochemistry, University of Wisconsin–Madison, 433 Babcock Drive, Madison, Wisconsin 53706-1544, Telephone: 608-262-8588, Fax: 608-890-2583, rtraines@wisc.edu.
[§]Current address: Janelia Farm Research Campus, Howard Hughes Medical Institute, 19700 Helix Drive, Ashburn, VA 20147.

[1]Abbreviations used: CHO, Chinese hamster ovary; DRNG RNase A, D38R/R39D/N67R/G88R variant of RNase A; GAG, glycosaminoglycan; ONC, Onconase® (a registered trademark of Tamir Biotechnology) or ranpirnase; PBS, phosphate-buffered saline; RFU, relative fluorescence units; RI, ribonuclease inhibitor; RNase A, bovine pancreatic ribonuclease; D-*threo*-PPMP, D-*threo*-1-phenyl-2-palmitoylamino-3-morpholino-1-propanol.

K_d value of the RI·RNase A complex and a concomitant gain in cytotoxicity (11). RNase A is less immunogenic than ONC (12), and DRNG RNase A has greater cancer-cell selectivity than ONC (11). Accordingly, mammalian ribonucleases are promising chemotherapeutic agents.

The general pathway by which ribonucleases mediate cytotoxicity appears to consist of cell-surface binding/association, internalization, endosomal escape, and cleavage of cytosolic RNA (13,14). Efficient cellular uptake is a prime determinant of ribonuclease cytotoxicity (15). As both DRNG RNase A and ONC are highly cationic proteins, adsorptive endocytosis rather than receptor-mediated endocytosis has been proposed as the mechanism of internalization (16).

Several lines of evidence suggest that non-specific Coulombic forces play a role in the association of ribonucleases with the cell surface. For example, RNase A and ONC bind to the cell surface in a nonsaturable manner (17). Condensing carboxyl groups with ethylenediamine increases the net charge of RNase A as well as its cytotoxicity (18,19). Similarly, cationization of ONC, its homologue cSBL, and RNase A by site-directed mutagenesis enhances internalization and cytotoxicity (20–22).

The toxicity of certain ribonucleases is highly specific for cancer cells *in vitro* and *in vivo* (23), but the underlying mechanism for this preference is unclear. The specificity has been attributed to unusual intracellular trafficking patterns, a high metabolic state, and the activation of pro-apoptotic pathways that are present in malignant cells but not normal cells (24–26). There is another hypothesis. Cancer cells are known to have altered cell-surface molecules and lipid-bilayer composition. Elevated levels of carboxylate- and sulfate-containing carbohydrates are observed frequently on cancer-cell surfaces (27), along with increased phosphatidylserine content in the outer leaflet of the plasma membrane (28). As a result, the surface of cancer cells is often more anionic than that of normal cells (29).

We sought to identify molecules on the surface of mammalian cells that mediate the uptake of mammalian ribonucleases. We did so by analyzing the binding of RNase A to glycans both *in vitro* and *in cellulo*. Although RNase A and ONC share a similar structure and net charge, we observed marked and unexpected differences regarding their cellular uptake. These results shed new light on the biochemical mechanism of ribonuclease-mediated cytotoxicity.

EXPERIMENTAL PROCEDURES

Materials

Escherichia coli strains BL21 (DE3) was from Novagen (Madison, WI). [*methyl*-^{3}H]Thymidine (6.7 Ci/mmol) was from Perkin Elmer (Boston, MA). *Clostridium perfringens* neuraminidase was from New England Biolabs (Ipswich, MA). *Staphylococcus aureus* strain V8 protease was from Sigma Aldrich (St. Louis, MO). D-*threo*-1-Phenyl-2-palmitoylamino-3-morpholino-1-propanol–HCl (D-*threo*-PPMP) was from Matreya (Pleasant Gap, PA). All other chemicals and reagents were of commercial reagent grade or better, and were used without further purification.

Mammalian cell lines

CHO-K1, CHO-677 (pgsD-677), CHO-745 (pgsA-745), Pro 5, Lec 2 cells were obtained from the American Type Culture Collection (Manassas, VA). CHO cell lines were grown in F12 medium. Pro 5 cells were grown in α-MEM with ribonucleosides and deoxyribonucleosides. Lec 2 cells were grown in α-MEM. All media for mammalian cell culture contained FBS (10% v/v), penicillin (100 units/mL), and streptomycin (100 μg/mL).

Cell-culture media and supplements were from Invitrogen (Carlsbad, CA). Cells were cultured at 37 °C in a humidified incubator containing CO_2(g) (5% v/v).

Instrumentation

Molecular mass was measured by MALDI TOF mass spectrometry using sinapinic acid as a matrix with a Voyager-DE-PRO Biospectrometry Workstation (Applied Biosystems, Foster City, CA) in the University of Wisconsin Biophysics Instrumentation Facility. Radioactivity was quantified by scintillation counting using a Microbeta TriLux liquid scintillation counter (Perkin Elmer, Boston, MA). Flow cytometry data were collected in the University of Wisconsin Paul P. Carbone Comprehensive Cancer Center with a FACSCalibur flow cytometer equipped with a 488-nm argon-ion laser (Becton Dickinson, Franklin Lakes, NJ). Microscopy images were obtained with a Nikon C1 laser scanning confocal microscope with a 60× oil immersion objective with NA 1.4. The zeta potential of cells was measured with a Malvern Zetasizer 3000HS dynamic light scattering instrument (Malvern, Worcestershire, UK).

Purification of ribonucleases

Ribonucleases were produced in *E. coli* strain BL21(DE3) and purified as described previously (7). Following purification, protein solutions were dialyzed against PBS and filtered (0.2-μm pore size) prior to use. Protein concentrations were determined by UV spectroscopy using extinction coefficients of $\varepsilon_{280} = 0.87\ (\text{mg}\cdot\text{mL}^{-1})^{-1}\cdot\text{cm}^{-1}$ for ONC and $\varepsilon_{278} = 0.72\ (\text{mg}\cdot\text{mL}^{-1})^{-1}\cdot\text{cm}^{-1}$ for RNase A.

Fluorophore labeling of ribonucleases

DRNG A19C RNase A and S61C ONC contain free cysteine residues for site-specific conjugation. During their purification, the free thiol groups were protected by reaction with 5,5′-dithio-bis(2-nitrobenzoic acid) (DTNB). Immediately prior to latent-fluorophore attachment, TNB-protected ribonucleases were deprotected with a four-fold excess of dithiothreitol and desalted by chromatography on a PD-10 column (GE Biosciences, Piscataway, NJ). A maleimido-containing latent fluorophore (**1**) was synthesized as described previously (30). Deprotected ribonucleases were reacted for 6 h at 25 °C with a ten-fold molar excess of latent fluorophore **1** (Figure 1B) (30). Conjugates were purified by chromatography using a HiTrap SP HP cation-exchange column (GE Biosciences, Piscataway, NJ). The molecular masses of ribonuclease conjugates were confirmed by MALDI TOF mass spectrometry. Protein concentration was determined by using a bicinchoninic acid (BCA) assay kit (Pierce, Rockford, IL) with wild-type RNase A as a standard.

Heparin-affinity chromatography

The affinity of ribonuclease for heparin was assessed *in vitro*. DRNG RNase A and ONC were mixed in a 1:1 ratio (1.0 mg each) in PBS at pH 7.2. This mixture was loaded onto a 1.0-mL HiTrap Heparin HP column (GE Healthcare, Piscataway, NJ). The column was washed with PBS, and ribonucleases were eluted with a linear gradient of NaCl (0.00–0.45 M) in PBS. Elution was monitored by absorbance at 280 nm, and eluted proteins were identified by mass spectrometry.

Flow cytometry

The cellular internalization of ribonucleases was followed by monitoring the unmasking of a pendant latent fluorophore by intracellular esterases (31). CHO cells from near confluent flasks were detached with a non-enzymic cell-dissociation solution (Sigma Aldrich, St. Louis, MO), collected by centrifugation, and resuspended at a density of 1×10^6 cells/mL in

fresh F12 media containing FBS (10% v/v). Labeled or unlabeled ribonucleases (10 μM) were added to 250 μL of F12/FBS containing 1 × 106 cells/mL of CHO cells. Samples were then allowed to incubate with ribonucleases at 37 °C for varying times. To quench internalization, CHO cells were collected by centrifugation at 1,000 rpm for 5 min at 4 °C, washed once with ice-cold PBS, and resuspended with 250 μL of PBS. Samples remained on ice until analyzed by flow cytometry.

Fluorescence was detected through a 530/30-nm band-pass filter. Cell viability was determined by staining with propidium iodide, which was detected through a 660-nm long-pass filter. The mean channel fluorescence intensity of 20,000 viable cells was determined for each sample with CellQuest software and used for subsequent analyses. To determine the steady-state rate constant for ribonuclease internalization, fluorescence intensity data were fitted to eq 1, in

$$F = F_{max}(1 - e^{-k_I t}) \quad (1)$$

which F_{max} is the fluorescence intensity upon reaching the steady-state and k_I is the first-order rate constant for ribonuclease internalization into CHO cells.

Zeta potential measurements

The zeta potential (ζ) of cells, which is a measure of their net charge, was determined by assessing their electrophoretic mobility in a fixed electric field (19 V/cm). This electrophoretic mobility is related to zeta potential by eq 2, in which μ is

$$\mu = \frac{\varepsilon \varsigma}{4\pi\eta} \quad (2)$$

electrophoretic mobility, and ε and η are the dielectric constant and viscosity of the solution, respectively. CHO cells in a near-confluent culture were detached from flasks by using a non-enzymatic cell-dissociation solution. The cells were collected by centrifugation at 1,000 rpm for 5 min, washed once with PBS (pH 7.0), and resuspended at a density of 3×10^4 cells/mL. Cells were then passed through a 40-μm nylon cell strainer immediately prior to use. The instrument was calibrated with a Zeta Potential Transfer Standard solution (ζ = −50 ± 5 mV). Electrophoretic mobility was determined by measurements for 15 min at 25 °C with 3 mL of cell suspension. Values of ζ are the mean (±SE) from at least three independent experiments with at least five measurements each.

Immunofluorescence microscopy

The binding of ribonucleases to cells was visualized by immunofluorescence microscopy. CHO cells were plated on coverslips placed in six-well plates 18–24 h before the experiment at a density of 5×10^5 cells/well. The next day, cells were washed twice with ice-cold medium, resuspended in 800 μL of medium containing FBS (10% v/v), followed by addition of a ribonuclease to 10 μM. The plate was then incubated on ice for 30 min. Samples were washed three times with medium containing FBS (10% v/v) and fixed with paraformaldehyde (4% v/v) for 20 min at 4 °C to prevent endocytosis. Following fixation, cells were washed five times with PBS containing Ca^{2+}/Mg^{2+} (1 mM each) and Tween 20 (0.1% v/v). Cell-surface associated ribonucleases were detected with a primary antibody (1 μg/mL), and fluorophore-labeled secondary antibody (1:1000 dilution). Coverslips were mounted on microscopy slides with MOWIOL 4-88 (Calbiochem, Gibbstown, NJ) and stored at 4 °C until analysis by confocal microscopy.

Cytotoxicity assays

The effect of a ribonuclease on the proliferation of CHO cells was assayed as described previously (7,11). After a 44-h incubation with DRNG RNase A or ONC, cells were treated with [*methyl*-^{3}H]thymidine for 4 h, and the incorporation of radioactive thymidine into cellular DNA was quantitated by liquid scintillation counting. The results are reported as the percentage of [*methyl*-^{3}H]thymidine incorporated relative to control cells. Data are the average of three measurements for each concentration, and the entire experiment was repeated in triplicate. Values of IC_{50}, which is the concentration of ribonucleases that decreases cell proliferation to 50%, were calculated by fitting the data using nonlinear regression to a sigmoidal dose–response curve, eq 3, in which *y* is the DNA synthesis following the [*methyl*-^{3}H]thymidine pulse and *h* is the slope of the curve.

$$y = \frac{100\%}{1 + 10^{(\log(IC_{50}) - \log[\text{ribonuclease}])h}} \quad (3)$$

RESULTS

Interaction with glycosaminoglycans

Glycosaminoglycans (GAGs) are long unbranched polysaccharides consisting of repeating disaccharide units (32). As cell-surface GAGs are highly heterogeneous, we first sought to determine if RNase A and ONC interact with heparin, which is a relatively homogeneous mimic of the GAGs on the surface of a mammalian cell (33,34). To minimize the effect of non-specific Coulombic interactions, we employed the cytotoxic DRNG variant of RNase A, which has the same the net charge (Z = +6) as wild-type ONC. We were surprised to find that, despite having an identical charge, ONC had markedly less affinity for heparin than did DRNG RNase A (Figure 1A). Likewise, the affinity of ONC for oligonucleotides is <1% that of RNase A (35), suggesting that ONC is deficient relative to RNase A in its ability to interact with a variety of anionic biopolymers.

Next, we sought to discover whether this difference in the mammalian and amphibian ribonucleases is replicated on the cell surface. To do so, we employed CHO-745 cells, which have defects in xylosyltransferase and are thus deficient in both heparan sulfate and chondroitin sulfate on the cell surface (36). The internalization of ribonucleases into wild-type and mutant cells was assessed by conjugation to latent fluorophore **1**, which become fluorescent only upon hydrolysis by intracellular esterases (Figure 1B) (30,31).

Initially, we visualized internalization by live-cell confocal microscopy. DRNG RNase A was internalized to a much higher level by wild-type (CHO-K1) cells (Figure 1C, panel i) than by mutant (CHO-745) cells (panel ii), suggesting the glycaosaminoglycans play a role in its uptake. By contrast, the level of ONC uptake was similar in CHO-K1 (panel iii) and CHO-745 cells (panel iv), and was much lower than that of DRNG RNase A.

Then, we examined the kinetics of internalization by using flow cytometry. The cellular uptake of DRNG RNase A was linear for the first 2 h and then approached a steady-state level (Figure 1D). The fluorescence intensity in the steady-state was dependent on the dose of DRNG RNase A up to 10 μM (data not shown), indicating that cell-surface binding sites are not saturable. Apparently, though, the ribonuclease-binding sites can be depleted after hours of continuous internalization, and this depletion leads to a steady state. The decrease in uptake rate was specific for DRNG RNase A, as the rate of uptake for endocytic markers such as transferring was constant for 6 h (data not shown). Finally, CHO cells did not show signs of apoptosis or enhanced propidium iodide staining after 6 h of incubation. Wild-type

RNase A, which is not cytotoxic, exhibited the same pattern as the cytotoxic variant DRNG RNase A, but at a lower steady-state level (data not shown).

We analyzed the uptake of DRNG RNase A by CHO cells quantitatively. Fitting the data in Figure 1D to eq 1 gives an uptake $t_{1/2} = \ln 2/k_I = 100$ and 120 min for CHO-K1 and CHO-745 cells, respectively, values comparable to those for the uptake of RNase 1 by K562 cells (20). The initial rate of DRNG RNase A uptake by CHO-K1 cells (220 ± 30 RFU h^{-1} at 10 μM) is ~4-fold greater than that by CHO-745 cells (60 ± 20 RFU h^{-1}). Similarly, the steady-state level attained by CHO-K1 cells is ~4-fold greater than by CHO-745 cells. As the fluid-phase endocytic rate as measured with dextran is comparable for these cell lines (data not shown), these results imply that heparan sulfate and chondroitin sulfate play key roles in mediating RNase A uptake.

In contrast to DRNG RNase A, the internalization rate of ONC is similar in CHO-K1 and CHO-745 cells (Figure 1E), suggesting that these GAGs are not involved in ONC uptake. Moreover, the initial rate of ONC uptake by CHO-K1 cells (4.1 ± 0.2 RFU h^{-1} at 10 μM) is ~50-fold less than that of DRNG RNase A uptake, and only slightly above the rate of fluid-phase uptake. These data are in gratifying agreement with the biochemical analyses of heparin-binding by DRNG RNase A and ONC (Figure 1A). The disparate rates and modes of RNase A and ONC uptake also indicate that these homologous proteins bind distinctly to the cell surface and could avail distinct internalization mechanisms.

Cellular binding and cell-surface charge

Most GAGs are polyanionic. Heparan sulfate, in particular, contains a high density of anionic functional groups—four per disaccharide unit (32). Together with sialic acid (37), these anionic carbohydrate moieties constitute the majority of cell-surface charge. To characterize further the relationship between cell-surface charge and ribonuclease binding, we employed other mutant cells with GAG deficiencies. CHO-677 cells lack heparan sulfate and produce 3-fold more chondroitin sulfate than do CHO-K1 cells (38,39). We determined the relative cell-surface charges of the wild-type and mutant CHO cells from their electrophoretic mobility (μ). By eq 2, the value of μ is related directly to the zeta potential (ζ), which in turn correlates with the surface charge density (σ) by a form of the Gouy Chapman equation (40):

$$\sigma = 13,410[1+(1-\alpha)^{1/2}]\sinh(\zeta/51.3) \quad (4)$$

where α refers to the fraction of the surface that is unavailable to counterions. As listed in Table 1, CHO-K1 cells, which have the most complete complement of GAGs, have the largest μ values, followed by CHO-677 cells, and then CHO-745 cells. Likewise, as shown in Figure 2A–C, the amount of DRNG RNase A bound to the cell surface decreases in the order: CHO-K1 > CHO-677 > CHO-745. Unlike with DRNG RNase A, ONC binding is similar to each of the three CHO cell lines (Figure 2D–F).

Uptake by Pro 5 and Lec 2 cells

Sialic acid is a common terminal residue of glycolipids, and *N*- and *O*-linked glycans (37). Elevated levels of sialic acid on the cell surface have been associated with numerous types of tumors as a result of increased activities of *N*-acetylglycosaminyltransferase V and upregulation of sialyltransferases (27). To determine if cell-surface sialic acid mediates the internalization of ribonucleases, we compared DRNG RNase A and ONC uptake by sialic acid-deficient cells. Lacking the ability to translocate CMP-sialic acid across Golgi membranes, Lec 2 cells have a 90% reduction in the sialylation of glycoproteins and

gangliosides compared with Pro 5 cells (41,42). The kinetic profiles of ribonuclease uptake by these cell lines are shown in Figure 3. Similar to the CHO cells, internalization of DRNG RNase A into Pro 5 and Lec 2 cells approach steady-state levels. The uptake by Pro 5 and Lec 2 cells has $t_{1/2}$ = 131 and 102 min, respectively, with Pro 5 cells reaching a higher steady-state level than Lec 2 cells. These $t_{1/2}$ values are comparable to those of CHO cells, which is consistent with a similar uptake mechanism by these cell lines. Notably, however, the difference in steady-state levels is smaller than expected—by 6 h, Pro 5 cells are only 1.8-fold more fluorescent than are Lec 2 cells, even though the difference in cell-surface sialic acid content is 10-fold. This dichotomy suggests that only a small fraction of cell-surface sialic acid is involved in DRNG RNase A internalization; most of the sialic acids are either not bound by the enzyme or do not lead to efficient uptake. ONC uptake, on the other hand, does not depend on sialic acids, as initial rates are indistinguishable in Pro 5 and Lec 2 cells (Figure 3B). Again, the rate and magnitude of ONC uptake is in drastic contrast to that of DRNG RNase A.

Uptake by treated cells

Using the paired cell lines, we have shown that multiple cell-surface moieties can mediate the uptake of RNase A. To investigate further the relative contribution of cell-surface molecules to ribonuclease uptake, we monitored internalization of DRNG RNase A and ONC into cells that had been treated chemically or enzymatically to remove or modify certain classes of cell-surface molecules. First, cell-surface gangliosides were depleted by treating cells with D-*threo*-PPMP, a specific inhibitor of glucosylceramide synthase, which catalyzes the first glucosylation step in the synthesis of all glucosylceramide-based glycosphingolipids (43,44). As shown in Figure 4, treatment with D-*threo*-PPMP (1 μM) for 7 days did not have an effect on the uptake of DRNG RNase A or ONC by CHO-K1 cells. (High levels of D-*threo*-PPMP (≤10 μM) were not notably cytotoxic; data not shown.) As CHO-K1 cells display predominantly the ganglioside GM3 (45), this finding indicates that GM3 is not a mediator of ribonuclease uptake. Second, protease-treated CHO-K1 cells exhibited an 80 and 60% reduction in DRNG RNase A and ONC uptake, respectively. Based on the data with mutant CHO cells, the proteins that mediate DRNG RNase A uptake are likely to be anionic cell-surface proteins, including proteoglycans containing heparan sulfate and chondroitin sulfate. Although ONC uptake was also decreased significantly after treatment with a protease, cell-surface proteins that mediate ONC internalization are likely to differ from those that mediate the uptake of DRNG RNase A. Hence, ONC could be interacting nonspecifically with a broad spectrum of cell-surface proteins, some of which lead to internalization and account for the majority of ONC uptake by CHO-K1 cells. Finally, treatment with a neuraminidase resulted in a 30 and 10% reduction in DRNG RNase A and ONC uptake, respectively. Sequential treatement with a protease and neuraminidase gave similar results, as did treatment with a protease alone (data not shown). Apparently, the sialic acids bound by ribonucleases are components of glycoproteins rather than glycolipids, corroborating the results from D-*threo*-PPMP treatment. In conclusion, cell-surface proteoglycans and glycoproteins mediate ribonuclease uptake, whereas glycolipids do not.

Cytotoxicity of ribonucleases

To evaluate the toxicity of DRNG RNase A and ONC, we measured the proliferation of the CHO, Pro 5, and Lec 2 cells in the presence of ribonucleases. The results are listed as IC_{50} values in Table 2. For DRNG RNase A, the IC_{50} value for CHO-745 cells is 1.5-fold that for CHO-K1 cells; likewise, the IC_{50} value for Lec 2 cells is 1.5-fold that for Pro 5 cells. Although the differences in cytotoxicity do not correlate directly with the steady-state levels attended by DRNG RNase A, a trend was observed—cell lines that internalized more ribonuclease were more vulnerable to their cytotoxic activity. KDRNG RNase A is another cytotoxic variant that contains an additional, K7A, substitution, and has biochemical

attributes similar to DRNG RNase A but one less charge at neutral pH (11). As listed in Table 2, the IC_{50} values of KDRNG RNase A also correlated with internalization. On the contrary, ONC displayed strikingly low IC_{50} values that range from ⅛ to $^{1}/_{45}$ those of DRNG RNase A, even though its uptake was much less than that of DRNG RNase A. Apparently, internalized ONC is a more efficient cytotoxin than is internalized DRNG RNase A.

DISCUSSION

RNase A and ONC are homologous ribonucleases. We have characterized relevant cell-surface interactions of these ribonucleases *in vitro* by using heparin-affinity chromatography, as well as *in cellulo* by monitoring binding and internalization (Figures 1–4). The use of mutant cell lines permitted us to assess the relationship between cell-surface charge and ribonuclease binding and internalization. The resulting data revealed insights into a potential tumor targeting mechanism for mammalian ribonucleases, as well as differences in the interaction of the amphibian and mammalian ribonuclease with human cells.

By quantifying the internalization of DRNG RNase A and ONC into a panel of cell lines, we find that DRNG RNase A is taken up by cells much more rapidly than is ONC. The kinetic profile of DRNG RNase A uptake is non-linear, and approaches a steady-state level after 3 h of incubation (Figure 1D). For human pancreatic ribonuclease (RNase 1), the establishment of a steady-state level had been thought to be due to lysosomal degradation of ribonucleases (31). Yet, RNase A variants are now known to resist proteolysis for up to 54 h in K562 cells (15). We also found that little or no loss of fluorescence occurred if RNase A conjugates were removed from the medium during the last 3 h of incubation (data not shown). Hence, lysosomal degradation cannot account for the decrease in the rate of internalization. Instead, we suspect that the rapid uptake depletes cell-surface binding sites and subsequent internalization, resulting in a gradual diminution of the rate constant over the time course. In contrast, the depletion of binding sites for ONC is insignificant, and ONC maintains a constant uptake rate (Figure 1E).

Endocytosis is a complex, multi-step process requiring the precise coordination of numerous molecules. When endocytosis is dissected into a series of kinetic events, the dynamics of cell-surface association and the mechanism of uptake are often reflected in measured kinetic parameters. In the present study, the internalization of DRNG RNase A at 10 μM can be approximated by a first-order kinetics model (eq 1) with rate constants of $k_I = 0.41 \pm 0.07$ h^{-1} and 0.32 ± 0.05 h^{-1} for CHO-K1 and Pro 5 cells, respectively. Kinetic analyses of RNase A uptake at additional concentrations (2 and 5 μM; data not shown) yielded a similar rate constant, as expected from this model. Similar to RNase A, the internalization of cell-penetrating peptides such as Tat has also been described by first-order kinetics (46), consistent with a common uptake mechanism. From reported time-course data (47), we estimate the rate constant for Tat uptake by CHO-K1 cells to be 1.2 h^{-1}. Although both Tat and RNase A interact with GAGs (48), the uptake rate of Tat into CHO-K1 cells is 3-fold higher than that of DRNG RNase A. The greater uptake rate exhibited by Tat could be due to a higher positive charge-to-mass ratio, which leads to a more favorable interaction with the anionic cell surface and thus faster uptake.

In contrast to DRNG RNase A, ONC is internalized at a constant rate for up to 10 h. Uptake of ONC (10 μM) by CHO-K1 and Pro 5 cells proceeded with initial rates of 4.1 ± 0.2 and 4.5 ± 0.2 RFU h^{-1}, respectively. A comparison of the uptakes rates of DRNG RNase A and ONC indicates that DRNG RNase A has a much more efficient internalization mechanism,

either due to higher affinity for the cell-surface or interaction with fast turnover cell-surface molecules. Although DRNG RNase A and ONC carry the same charge at physiological pH, DRNG RNase A has more arginine and lysine residues on its concave side, which could make favorable contacts with anionic cell-surface moieties. This hypothesis is consistent with the recent finding that the location of cationic residues is key to ONC internalization (22).

ONC uptake by CHO cells is only slightly faster than fluid-phase uptake. Our data with CHO cells suggest that ONC interacts minimally with cell-surface GAGs and sialic acids (Figures 1E and 3B). Yet, ONC does bind to the cell surface (Figure 2D–F). Treating CHO-K1 cells with a protease eliminated 56% of ONC uptake (Figure 4), suggesting that ONC associates with cell-surface glycoproteins. Hence, whereas RNase A targets abundant cell-surface proteoglycans and sialic acid-containing glycoproteins, ONC binds to glycoproteins that might not mediate productive internalization.

The cytotoxicity of ribonucleases is determined by the interplay of a number of factors, including conformational stability, catalytic ability, internalization, and affinity for mammalian RI (4). With the exception of some residual affinity for human RI, DRNG RNase A is superior to ONC as a cytotoxin by all known biochemical measures. It is thus surprising that ONC tends to have lower IC_{50} values than does DRNG RNase A (11). Steps downstream from internalization must account for the greater cytotoxicity of ONC. For example, while RNase A resides in acidic late endosomal/lysosomal compartments (17), ONC is in recycling endosomes, where the near neutral pH could facilitate ONC translocation (49). Ribonucleases must traverse a phospholipid bilayer to exert their ribonucleolytic activity, and ONC could be translocated more efficiently than RNase A. Once in the cytosol, ONC degrades a broad range of RNA substrates (50−52), whereas the targets of RNase A are unknown and could be less fateful.

The toxicity exhibited by mammalian ribonucleases is specific for tumor cells (11). The basis for this specificity is unknown. As cancer cells frequently have more anionic surfaces than do their wild-type counterparts (29), the anionicity of the cell surface could be exploited by cationic ribonucleases as a means to target cancer cells. Herein, we have used mutant CHO cells to demonstrate a relationship between cell-surface charge and the internalization and toxicity of a mammalian ribonuclease (Figure 1D and 2A–C; Tables 1 and 2). Interestingly, a correlation between cell-surface charge and tumorigenicity is known among these same cell lines. CHO-K1 cells, with the most complete complement of cell-surface carbohydrates and highest μ value, have the highest frequency of tumor formation in nude mice, whereas CHO-677 and CHO-745 do not produce tumors (Table 1). Hence, our finding that the μ value of cells correlates directly with the cell-surface binding, internalization, and cytotoxicity of a mammalian ribonuclease is consistent with the therapeutic index arising, at least in part, from the targeting of the anionic cell-surface moieties that are especially abundant on tumor cells.

Unlike with RNase A, no correlation was apparent in the cell-surface binding, internalization, and cytotoxicity of ONC. We find that, for example, ONC does not distinguish between highly anionic cancerous cells (here, CHO-K1) and noncancerous cells (CHO-745). Evidently, this amphibian ribonuclease, which has clinical utility as an anticancer agent (4), does not target cancer cells by interacting with abundant anionic cell-surface glycans.

The cellular entry of a mammalian ribonuclease could have important biological implications. For example, Asn88, a key RI-contact site in human pancreatic ribonuclease (53), is known to be *N*-glycosylated in humans (54). The *N*-glycosylation of ONC increases

its toxicity for cancer cells, presumably by enhancing its stability *in cellulo* (55). Accordingly, an *N*-glycosylated human ribonuclease could evade RI and provide endogenous anti-tumor activity.

Acknowledgments

We are grateful to Professor Joel A. Pedersen (University of Wisconsin–Madison) for the use of his Malvern Zetasizer 3000HS dynamic light scattering instrument.

REFERENCES

1. Dan S, Tsunoda T, Kitahara O, Yanagawa R, Zembutsu H, Katagiri T, Yamazaki K, Nakamura Y, Yamori T. An integrated database of chemosensitivity to 55 anticancer drugs and gene expression profiles of 39 human cancer cell lines. Cancer Res. 2002; 62:1139–1147. [PubMed: 11861395]
2. Onyango P. The role of emerging genomics and proteomics technologies in cancer drug target discovery. Curr. Cancer Drug Targets. 2004; 4:111–124. [PubMed: 15032664]
3. Alvarez-Salas LM. Nucleic acids as therapeutic agents. Curr. Top. Med. Chem. 2008; 8:1379–1404. [PubMed: 18991725]
4. Lee JE, Raines RT. Ribonucleases as novel chemotherapeutics: The ranpirnase example. BioDrugs. 2008; 22:53–58. [PubMed: 18215091]
5. Raines RT. Ribonuclease A. Chem. Rev. 1998; 98:1045–1065. [PubMed: 11848924]
6. Dickson KA, Haigis MC, Raines RT. Ribonuclease inhibitor: Structure and function. Prog. Nucleic Acid Res. Mol. Biol. 2005; 80:349–374. [PubMed: 16164979]
7. Leland PA, Schultz LW, Kim B-M, Raines RT. Ribonuclease A variants with potent cytotoxic activity. Proc. Natl. Acad. Sci. USA. 1998; 98:10407–10412. [PubMed: 9724716]
8. Haigis MC, Kurten EL, Raines RT. Ribonuclease inhibitor as an intracellular sentry. Nucleic Acids Res. 2003; 31:1024–1032. [PubMed: 12560499]
9. Dickson KA, Raines RT. Silencing an inhibitor unleashes a cytotoxic enzyme. Biochemistry. 2009; 48:5015–5053.
10. Rutkoski TJ, Kink JA, Strong LE, Schilling CI, Raines RT. Antitumor activity of ribonuclease multimers created by site-specific covalent tethering. Bioconjug. Chem. 2010; 21:1691–1702. [PubMed: 20704261]
11. Rutkoski TJ, Kurten EL, Mitchell JC, Raines RT. Disruption of shape-complementarity markers to create cytotoxic variants of ribonuclease A. J. Mol. Biol. 2005; 354:41–54. [PubMed: 16188273]
12. Matoušek J, Souček J, Slavík T, Tománek M, Lee JE, Raines RT. Comprehensive comparison of the cytotoxic activities of onconase and bovine seminal ribonuclease. Comp. Biochem. Physiol. 2003; 136C:343–356.
13. Leland PA, Raines RT. Cancer chemotherapy—ribonucleases to the rescue. Chem. Biol. 2001; 8:405–413. [PubMed: 11358688]
14. Rutkoski TJ, Raines RT. Evasion of ribonuclease inhibitor as a determinant of ribonuclease cytotoxicity. Curr. Pharm. Biotechnol. 2008; 9:185–199. [PubMed: 18673284]
15. Leich F, Stohr N, Rietz A, Ulbrich-Hofmann R, Arnold U. Endocytotic internalization as a crucial factor for the cytotoxicity of ribonucleases. J. Biol. Chem. 2007; 282:27640–27646. [PubMed: 17635931]
16. Benito A, Ribó M, Vilanova M. On the track of antitumor ribonucleases. Mol. Biosyst. 2005; 1:294–302. [PubMed: 16880994]
17. Haigis MC, Raines RT. Secretory ribonucleases are internalized by a dynamin-independent endocytic pathway. J. Cell Sci. 2003; 116:313–324. [PubMed: 12482917]
18. Futami J, Kitazoe M, Maeda T, Nukui E, Sakaguchi M, Kosaka J, Miyazaki M, Kosaka M, Tada H, Seno M, Sasaki Y, Huh NH, Namba M, Yamada H. Intracellular delivery of proteins into mammalian living cells by polyethylenimine-cationization. J. Biosci. Bioeng. 2005; 99:95–103. [PubMed: 16233763]
19. Futami J, Yamada H. Design of cytotoxic ribonucleases by cationization to enhance intracellular protein delivery. Curr. Pharm. Biotechnol. 2008; 9:180–184. [PubMed: 18673283]

20. Ogawa Y, Iwama M, Ohgi K, Tsuji T, Irie M, Itagaki T, Kobayashi Hand, Inokuchi N. Effect of replacing the aspartic acid/glutamic acid residues of bullfrog sialic acid binding lectin with asparagine/glutamine and arginine on the inhibition of cell proliferation in murine leukemia P388 cells. Biol. Pharm. Bull. 2002; 25:722–727. [PubMed: 12081136]
21. Fuchs SM, Rutkoski TJ, Kung VM, Groeschl RT, Raines RT. Increasing the potency of a cytotoxin with an arginine graft. Protein Eng. Des. Select. 2007; 20:505–509.
22. Turcotte RF, Lavis L, Raines RT. Onconase cytotoxicity relies on the ditribution of its positive charge. FEBS J. 2009; 276:4270–4281.
23. Arnold U, Ulbrich-Hofmann R. Natural and engineered ribonucleases as potential cancer therapeutics. Biotechnol. Lett. 2006; 28:1615–1622. [PubMed: 16902846]
24. Smith MR, Newton DL, Mikulski SM, Rybak SM. Cell cycle-related differences in susceptibility of NIH/3T3 cells to ribonucleases. Exp. Cell Res. 1999; 247:220–232. [PubMed: 10047464]
25. Iordanov MS, Wong J, Newton DL, Rybak SM, Bright RK, Flavell RA, Davis RJ, Magun BE. Differential requirement for the stress-activated protein kinase/c-Jun NH_2-terminal kinase in RNA damage-induced apoptosis in primary and in immortalized fibroblasts. Mol. Cell. Biol. Res. Commun. 2000; 4:122–128. [PubMed: 11170843]
26. Bracale A, Spalletti-Cernia D, Mastronicola M, Castaldi F, Mannucci R, Nitsch L, D'Alessio G. Essential stations in the intracellular pathway of cytotoxic bovine seminal ribonuclease. Biochem. J. 2002; 362:553–560. [PubMed: 11879181]
27. Dube DH, Bertozzi CR. Glycans in cancer and inflammation—potential for therapeutics and diagnostics. Nat. Rev. Drug Discov. 2005; 4:477–488. [PubMed: 15931257]
28. Ran S, Downes A, Thorpe PE. Increased exposure of anionic phospholipids on the surface of tumor blood vessels. Cancer Res. 2002; 62:6132–6140. [PubMed: 12414638]
29. Slivinsky GG, Hymer WC, Bauer J, Morrison DR. Cellular electrophoretic mobility data: A first approach to a database. Electrophoresis. 1997; 18:1109–1119. [PubMed: 9237565]
30. Lavis LD, Chao T-Y, Raines RT. Fluorogenic label for biomolecular imaging. ACS Chem. Biol. 2006; 1:252–260. [PubMed: 17163679]
31. Johnson RJ, Chao T-Y, Lavis LD, Raines RT. Cytotoxic ribonucleases: The dichotomy of Coulombic forces. Biochemistry. 2007; 46:10308–10316. [PubMed: 17705507]
32. Laremore TN, Zhang F, Dordick JS, Liu J, Linhardt RJ. Recent progress and applications in glycosaminoglycan and heparin research. Curr. Opin. Chem. Biol. 2009; 13:633–640. [PubMed: 19781979]
33. Fuchs SM, Raines RT. Pathway for polyarginine entry into mammalian cells. Biochemistry. 2004; 43:2438–2444. [PubMed: 14992581]
34. Varki, A.; Cummings, RD.; Esko, JD.; Freeze, HH.; Stanley, P.; Hart, G.; Etzler, ME. Essentials of Glycobiology. 2nd Ed.. Cold Spring Harbor, NY: Cold Spring Harbor Laboratory Press; 2008.
35. Lee JE, Raines RT. Contribution of active-site residues to the function of onconase, a ribonuclease with antitumoral activity. Biochemistry. 2003; 42:11443–11450. [PubMed: 14516195]
36. Esko JD, Stewart TE, Taylor WH. Animal cell mutants defective in glycosaminoglycan biosynthesis. Proc. Natl. Acad. Sci. USA. 1985; 82:3197–3201. [PubMed: 3858816]
37. Chen X, Varki A. Advances in the biology and chemistry of sialic acids. ACS Chem. Biol. 2010; 5:163–176. [PubMed: 20020717]
38. Lidholt K, Weinke JL, Kiser CS, Lugemwa FN, Bame KJ, Cheifetz S, Massague J, Lindahl U, Esko JD. A single mutation affects both *N*-acetylglucosaminyltransferase and glucuronosyltransferase activities in a Chinese hamster ovary cell mutant defective in heparan sulfate biosynthesis. Proc. Natl. Acad. Sci. USA. 1992; 89:2267–2271. [PubMed: 1532254]
39. Norgard-Sumnicht K, Bai XM, Esko JD, Varki A, Manzi AE. Exploring the outcome of genetic modifications of glycosylation in cultured cell lines by concurrent isolation of the major classes of vertebrate glycans. Glycobiology. 2000; 10:691–700. [PubMed: 10910973]
40. Mehrishi JN. Molecular aspects of the mammalian cell surface. Prog. Biophys. Mol. Biol. 1972; 25:1–70. [PubMed: 4122510]
41. Stanley P, Sudo T, Carver JP. Differential involvement of cell surface sialic acid residues in wheat germ agglutinin binding to parental and wheat germ agglutinin-resistant Chinese hamster ovary cells. J. Cell Biol. 1980; 85:60–69. [PubMed: 7364875]

42. Deutscher SL, Nuwayhid N, Stanley P, Briles EIB, Hirschberg CB. Translocation across Golgi vesicle membranes: A CHO glycosylation mutant deficient in CMP-sialic acid transport. Cell. 1984; 39:295–299. [PubMed: 6498937]
43. Li RX, Manela J, Kong Y, Ladisch S. Cellular gangliosides promote growth factor-induced proliferation of fibroblasts. J. Biol. Chem. 2000; 275:34213–34223. [PubMed: 10859325]
44. Zurita AR, Maccioni HJF, Daniotti JL. Modulation of epidermal growth factor receptor phosphorylation by endogenously expressed gangliosides. Biochem. J. 2001; 355:465–472. [PubMed: 11284735]
45. Crespo PM, Zurita AR, Giraudo CG, Maccioni HJ, Daniotti JL. Ganglioside glycosyltransferases and newly synthesized gangliosides are excluded from detergent-insoluble complexes of Golgi membranes. Biochem. J. 2004; 377:561–568. [PubMed: 14565845]
46. Zorko M, Langel U. Cell-penetrating peptides: Mechanism and kinetics of cargo delivery. Adv. Drug Deliv. Rev. 2005; 57:529–545. [PubMed: 15722162]
47. Jones SW, Christison R, Bundell K, Voyce CJ, Brockbank SMV, Newham P, Lindsay MA. Characterization of cell-penetrating peptide-mediated peptide delivery. Brit. J. Pharmacol. 2005; 145:1093–1102. [PubMed: 15937518]
48. Kosuge M, Takeuchi T, Nakase I, Jones AT, Futaki S. Cellular internalization and distribution of arginine-rich peptides as a function of extracellular peptide concentration, serum, and plasma membrane associated proteoglycans. Bioconjug. Chem. 2008; 19:656–664. [PubMed: 18269225]
49. Rodriguez M, Torrent G, Bosch M, Rayne F, Dubremetz J-F, Ribó M, Benito A, Vilanova M, Beaumelle B. Intracellular pathway of Onconase that enables its delivery to the cytosol. J. Cell Sci. 2007; 120:1405–1411. [PubMed: 17374640]
50. Wu Y, Mikulski SM, Ardelt W, Rybak SM, Youle RJ. A cytotoxic ribonuclease: Study of the mechanism of onconase cytotoxicity. J. Biol. Chem. 1993; 268:10686–10693. [PubMed: 8486718]
51. Iordanov MS, Ryabinina OP, Wong J, Dinh TH, Newton DL, Rybak SM, Magun BE. Molecular determinants of apoptosis induced by the cytotoxic ribonuclease onconase: Evidence for cytotoxic mechanisms different from inhibition of protein synthesis. Cancer Res. 2000; 60:1983–1994. [PubMed: 10766189]
52. Zhao H, Ardelt B, Ardelt W, Shogen K, Darzynkiewicz Z. The cytotoxic ribonuclease onconase targets RNA interference (siRNA). Cell Cycle. 2008; 7:3258–3261. [PubMed: 18927512]
53. Johnson RJ, Lin SR, Raines RT. Genetic selection reveals the role of a buried, conserved polar residue. Protein Sci. 2007; 16:1609–1616. [PubMed: 17656580]
54. Ribó M, Beintema JJ, Osset M, Fernández E, Bravo J, de Llorens R, Cuchillo CM. Heterogeneity in the glycosylation pattern of human pancreatic ribonuclease. Biol. Chem. Hoppe-Seyler. 1994; 375:357–363. [PubMed: 8074810]
55. Kim B-M, Kim H, Raines RT, Lee Y. Glycosylation of onconase increases it conformational stability and toxicity for cancer cells. Biochem. Biophys. Res. Commun. 2004; 315:976–983. [PubMed: 14985108]
56. Esko JD, Rostand KS, Weinke JL. Tumor formation dependent on proteoglycan biosynthesis. Science. 1988; 241:1092–1096. [PubMed: 3137658]

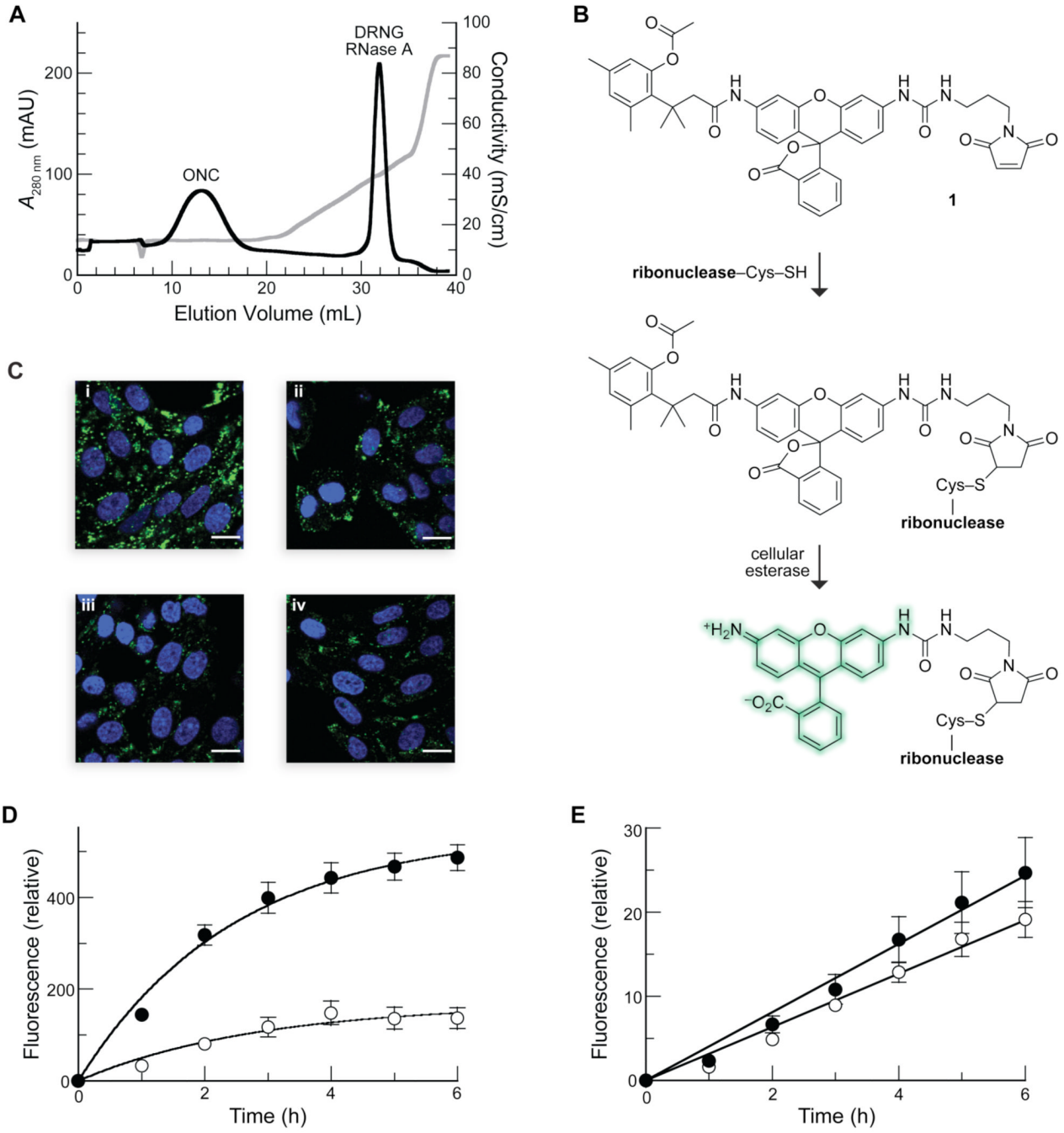

FIGURE 1.

Interaction of ribonucleases with GAGs *in vitro* and *in cellulo*. (A) Elution profile of DRNG RNase A and ONC from immobilized heparin. Ribonucleases (1.0 mg each) were loaded onto a column of immobilized heparin in PBS at pH 7.2. Protein elution was monitored by absorbance at 280 nm (black line) during a linear gradient of additional NaCl (0.00–0.45 M) (conductivity, grey line). ONC did not bind to heparin, eluting during the PBS wash (conductivity: 14 mS/cm). DRNG RNase A eluted at a conductivity of 40 mS/cm. (B) Scheme for the labeling of a ribonuclease with latent fluorophore **1**. (C) Uptake of labeled DRNG RNase A (10 μM; i and ii) and ONC (10 μM; iii and iv) by CHO-K1 (i and iii) and CHO-745 (ii and iv) cells after incubation for 6 h at 37 °C. Nuclear stain Hoechst 33342

(blue) was added for the last 5 min of incubation. Scale bar: 10 μm. (D and E) Kinetics of uptake of labeled DRNG RNase A (10 μM; D) and ONC (10 μM; E) by detached CHO-K1 (●) and CHO-745 (○) cells. Total cellular fluorescence was measured by flow cytometry. Data points are mean values (±SE) for 20,000 cells from ≥6 cell populations. Initial rates of DRNG RNase A uptake were 220 ± 30 and 60 ± 20 RFU h^{-1} for CHO-K1 and CHO-745 cells, respectively. Initial rates of ONC uptake were 4.1 ± 0.2 and 3.2 ± 0.1 RFU h^{-1} for CHO-K1 and CHO-745 cells, respectively.

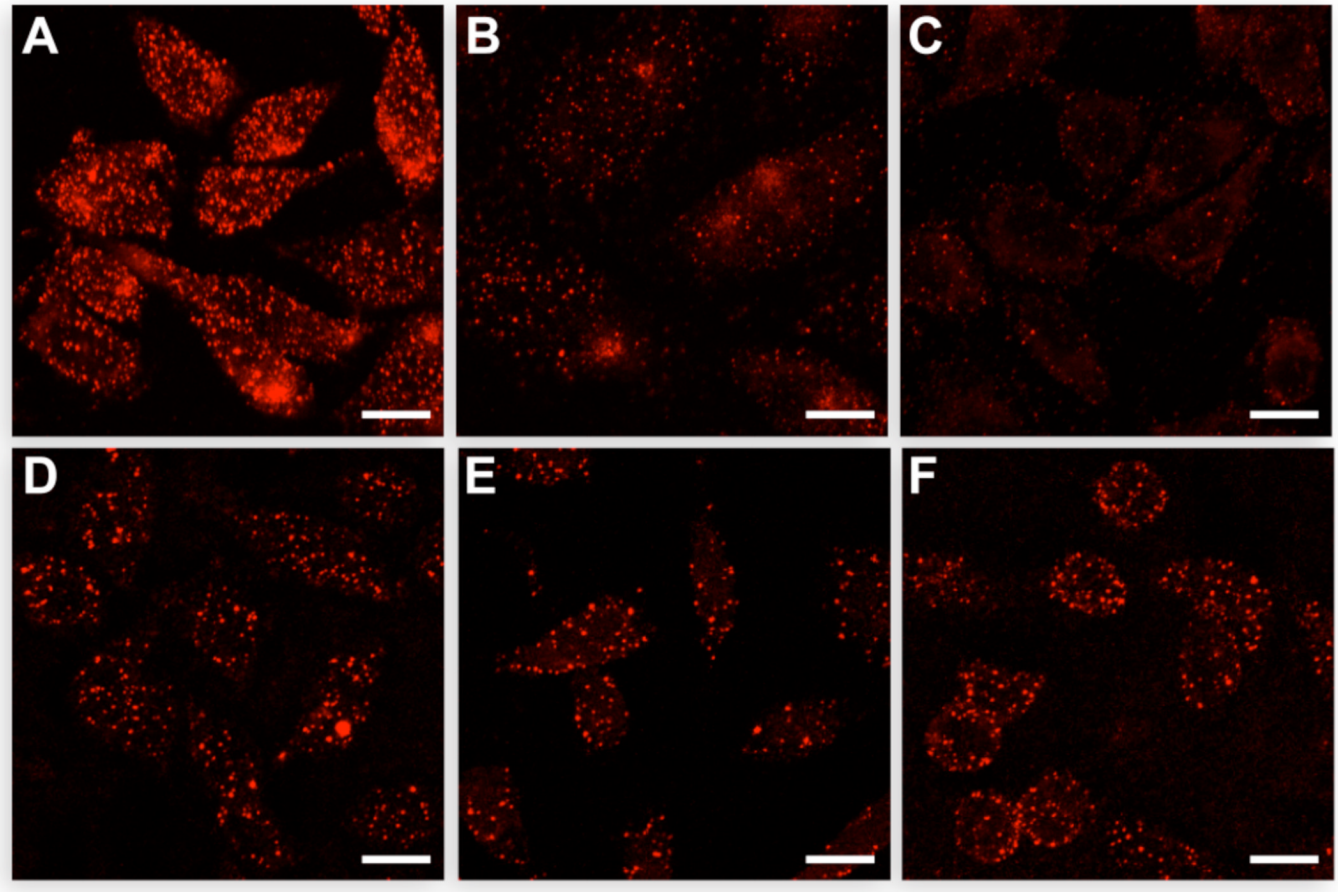

FIGURE 2.

Binding of ribonucleases to wild-type and GAG-deficient mammalian cells. DRNG RNase A (A–C) and ONC (D–F) were detected by using a primary antibody and fluorescent secondary antibody. A and D, CHO-K1 cells. B and E, CHO-677 cells. C and F, CHO-745 cells. Scale bar: 10 μm.

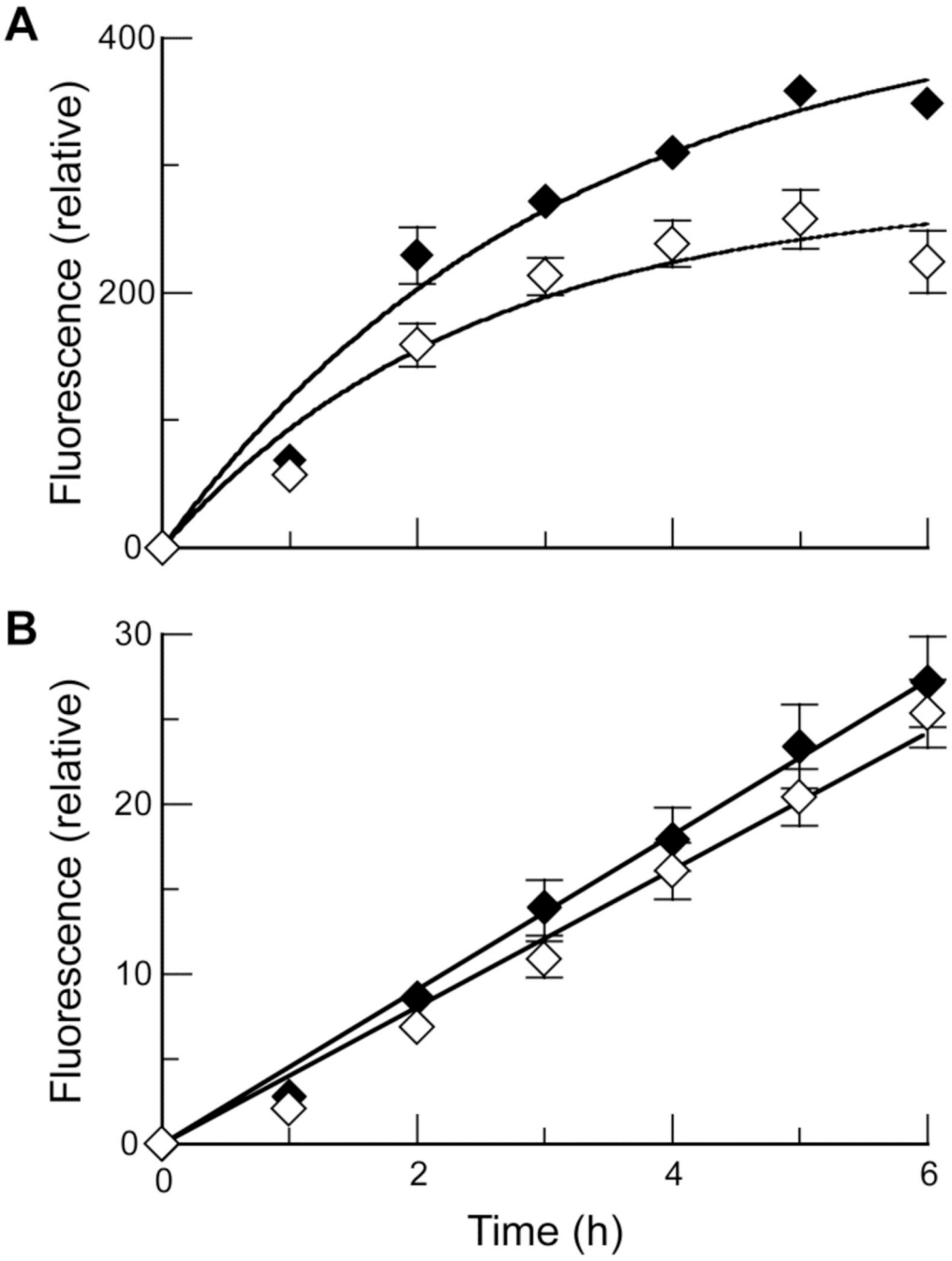

FIGURE 3.

Kinetics of ribonuclease uptake by wild-type and sialic acid-deficient mammalian cells. Labeled DRNG RNase A (10 μM; A) and ONC (10 μM; B) were incubated with detached Pro 5 (◆) and Lec 2 (◇) cells. Total cellular fluorescence was measured by flow cytometry. Data points are mean values (±SE) for 20,000 cells from ≥6 cell populations. Initial rates of DRNG RNase A uptake were 140 ± 20 and 110 ± 30 RFU h^{-1} for Pro 5 and Lec 2 cells, respectively. Initial rates of ONC uptake were 4.5 ± 0.2 and 4.0 ± 0.1 RFU h^{-1} for Pro 5 and Lec 2 cells, respectively.

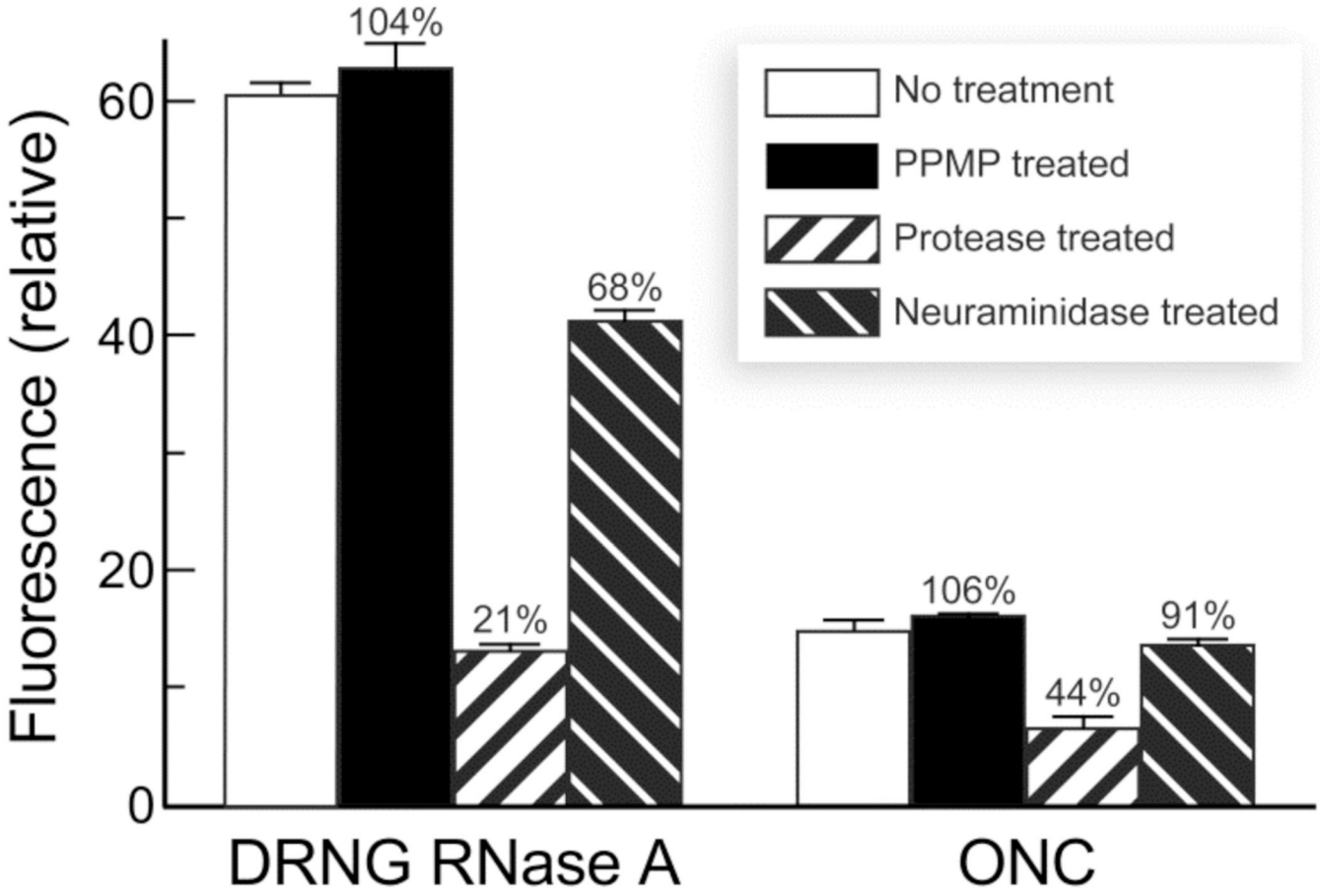

FIGURE 4.

Uptake of ribonucleases by chemical- or enzyme-treated mammalian cells. Labeled DRNG RNase A and ONC were incubated for 1 and 3 h, respectively, with CHO-K1 cells that had been treated with D-*threo*-PPMP, V8 protease, or neuraminidase. Total cell fluorescence was measured by flow cytometry. Values of fluorescence intensity are the mean (±SE) for 20,000 cells from ≥6 cell populations.

Table 1

Electrophoretic mobility and tumorigenicity of CHO cells

Cell line	Cell-surface GAG deficiency	μ ((μm/s)/(V/cm))[a]	Tumorigenicity[b]
CHO-K1	none	−1.5 ± 0.1	19/22
CHO-677	No heparan sulfate	−1.2 ± 0.1	0/7
CHO-745	No heparan sulfate No chondroitin sulfate	−1.08 ± 0.05	0/28

[a] Calculated with eq 2 from the value of ζ measured at pH 7.0.

[b] Based on ref. (56). Values indicate the frequency of tumor formation when 10^7 cells were injected subcutaneously into nude mice.

Table 2

Values of IC_{50} (μM) for cell proliferation in the presence of ribonucleases[a]

Cell line	ribonuclease		
	DRNG RNase A	KDRNG RNase A	ONC
CHO-K1	18.5 ± 0.1	20.1 ± 0.1	2.2 ± 0.1
CHO-745	27.1 ± 0.1	39.8 ± 0.03	0.6 ± 0.3
Pro 5	4.63 ± 0.09	8.79 ± 0.03	0.4 ± 0.1
Lec 2	6.7 ± 0.1	14.44 ± 0.04	0.6 ± 0.2

[a]Values of IC_{50} (±SE) are for incorporation of [*methyl*-^{3}H]thymidine into the DNA of cells treated with a ribonuclease.